# Influence of body mass on the shape of forelimb in musteloid carnivorans

ANNE-CLAIRE FABRE[1–3]*, RAPHAEL CORNETTE[4], STÉPHANE PEIGNÉ[1] and ANJALI GOSWAMI[3]

[1]*CR2P – UMR 7207 CNRS, MNHN, Univ Paris 06, 57 rue Cuvier, CP 38, F-75005, Paris, France*
[2]*Univ Paris Diderot, Paris, France*
[3]*Department of Genetics, Evolution, and Environment and Department of Earth Sciences, University College London, Darwin Building 118A, Gower Street, London WC1E 6BT, UK*
[4]*OSEB – UMR 7205 CNRS, MNHN, 45 Rue Buffon, F-75005, Paris, France*

In the majority of mammals, the limbs are positioned under the body and play an important role in gravitational support, allowing the transfer of the load and providing stability to the animal. For this reason, an animal's body mass likely has a significant effect on the shape of its limb bones. In the present study, we investigate the influence of body mass variation on the shape of the three long bones of the forelimb in a group of closely-related species of mammals: the musteloid carnivorans. We use geometric morphometric techniques to quantify forelimb shape; then estimate phylogenetic signal in the shape of each long bone; and, finally, we apply an independent contrasts approach to assess evolutionary associations between forelimb shape and body mass. The results obtained show that body mass evolution is tightly coordinated with the evolution of forelimb shape, although not equally in all elements. In particular, the humeral and radial shapes of heavier species appear better suited for load bearing and load transmission than the ulna. Nevertheless, our results also show that body mass influences only part of forelimb long bone shape and that other factors, such as locomotor ecology, must be considered to fully understand forelimb evolution. © 2013 The Linnean Society of London, *Biological Journal of the Linnean Society*, 2013, **110**, 91–103.

ADDITIONAL KEYWORDS: 3D geometric morphometrics – body size – comparative analysis – elbow joint – humerus – radius – ulna.

## INTRODUCTION

How body size affects the form of the vertebrate skeleton has long been a topic of interest for evolutionary biologists, comparative anatomists, and, more generally, natural scientists. The effect of body size on the form of the vertebrate skeleton was first documented by Galileo Galilei (1637) in *Dialogues*, in which he noted that the bones of larger and heavier animals tend to be thicker and more robust than those of smaller and lighter ones. Indeed, a large body size imposes biomechanical constraints on the animal, and its skeleton needs to minimally support its own weight without collapsing or breaking. Yet, as body mass increases to the third power relative to body length (Schmidt-Nielson, 1984), larger animals will have disproportionately greater forces acting on their limbs than smaller ones, resulting in the evolution of shorter and stockier bones with a greater cross-sectional area (Biewener, 1983). Moreover, larger animals are subjected to greater stresses and strains on their limb bones during locomotion (Biewener, 1989, 2005), further imposing constraints on the size and shape of the long bones of fore- and hindlimbs.

The biomechanical consequences of body size variation on the overall structure of the skeleton are relatively well studied (Rubin & Lanyon, 1982; Biewener, 1983, 1989; Thomason, 1985; Reynolds,

---

*Corresponding author. E-mail: acfabre@mnhn.fr

1985; Bertram & Biewener, 1990; Ruff & Runestad, 1992; Heinrich & Biknevicius, 1998; Christiansen, 1999; Blob & Biewener, 2001; Biewener, 2005; Day & Jayne, 2007). However, the effect of body size variation on the shape of the long bones of the limbs, and especially on their articulations, remains poorly understood.

In the present study, we focus on the influence of body mass variation on the shape of long bones of the forelimb in mammals. In the typical mammalian body plan, the forelimbs are positioned under the body and play a role in the support of the body. Indeed, the forelimbs play a role in gravitational support, allowing load transfer and providing stability to an animal (Jenkins, 1973; Evans, 1993). The effects of body mass variation can thus be expected to be especially noticeable at the level of the joints of the forelimb, such as the elbow articulation where forces are transferred from the humerus to the radius and ulna (Biewener, 1989, 2005).

To investigate the evolution of potential morphological adaptations of the forelimb in relation to body size, we present a quantitative morphological analysis of the three long-bones of the forelimb in a group of closely-related species: the musteloid carnivorans. The Musteloidea (Mephitidae, Ailuridae, Procyonidae, and Mustelidae) are a good model system for this type of study because they display a wide range of body sizes from very small to large, spanning three orders of magnitude with little or no change in limb posture. Indeed, the least weasel (*Mustela nivalis*) weighs approximately 26 g, whereas some sea otters (*Enhydra lutris*) can reach up to 45 kg in body mass. In addition, their phylogenetic relationships are well resolved (Sato *et al.*, 2009, 2012; Eizirik *et al.*, 2010): the mustelids (weasels, badgers, otters, and their relatives) and the procyonids (coatis, raccoons, the kinkajous, and their relatives) are sister taxa, whereas the ailurids (which is represented by a unique living representative, the red panda) and the mephitids (skunks) form successive sister lineages related to this clade (Fig. 1).

In the present study, we analyze the influence of the body mass on the shape of the forelimb using three-dimensional (3D) geometric morphometric methods, focusing specifically on the elbow articulation. We first estimate the phylogenetic signal in the shape of each long bone and then utilize independent contrast approaches (Felsenstein, 1985) to assess the correlation between forelimb shape and body mass. This approach allows us to: (1) quantify the influence of the evolution of a greater body mass on the evolution of forelimb long bone shape and (2) investigate the morphological adaptations related to body size for each long bone of the forelimb. Combined, these analyses will test the hypothesis that the shape of the

forelimb long bones and their articulations evolved under constraints imposed by body mass in musteloids. We predict that, as larger and heavier species will be subjected to larger forces on the elbow joint than smaller and lighter ones, the shape of the articular surfaces will be optimized to distribute and transmit the gravitational forces through an increase in joint surface area and overall contact area. Moreover, we predict the long bones of heavier species will be more robust, with a wider and shorter shaft relative to the overall shape of each bone.

## MATERIAL AND METHODS

### MATERIAL

Long bones of the forelimb (humerus, ulna and radius) from 78 individuals belonging to eight species of procyonids, one species of ailurid, four mephitids, and 20 mustelids were used in the present study. The number of specimens for each species ranged from one to seven individuals (Table 1). All specimens were adults and predominantly of wild caught origin. Equal numbers of males and females were included where possible. Forelimb bones were obtained from the several collections: Mammifères et Oiseaux, Muséum National d'Histoire Naturelle, Paris, France; the Naturhistorisches Museum, Basel, Switzerland; the Harvard Museum of Comparative Zoology, Cambridge, Massachusetts, and the Smithsonian National Museum of Natural History, Washington, District of Columbia, USA. A complete list of the specimens used in the analyses is provided in the Supporting information (Table S1). All the bones of the forelimb were digitized using a Breuckmann 3D surface scanner at the Muséum National d'Histoire Naturelle, Paris (white light fringe StereoSCAN³ᴰ model with a camera resolution of 1.4 megapixels).

### GEOMETRIC MORPHOMETRICS

Because of the complex shape of the elbow articulation, it cannot be fully represented using traditional landmarks. Thus, a 3D sliding-semilandmark procedure using surface landmarks was used to quantify the forelimb morphology of the specimens in the present study (Bookstein, 1997; Gunz, Mitteroecker & Bookstein, 2005). Through this procedure, sliding-semilandmarks on surfaces and curves are transformed into geometrically (i.e. spatially) homologous landmarks that can be used to compare shapes. Semilandmarks are allowed to slide along the curves and surfaces that are predefined at the same time as minimizing the bending energy. Landmarks and curves were obtained using IDAV LANDMARK (Wiley *et al.*, 2005), whereas EDGEWARP3D, version 3.31 (Bookstein & Green, 2002) was used to performed the
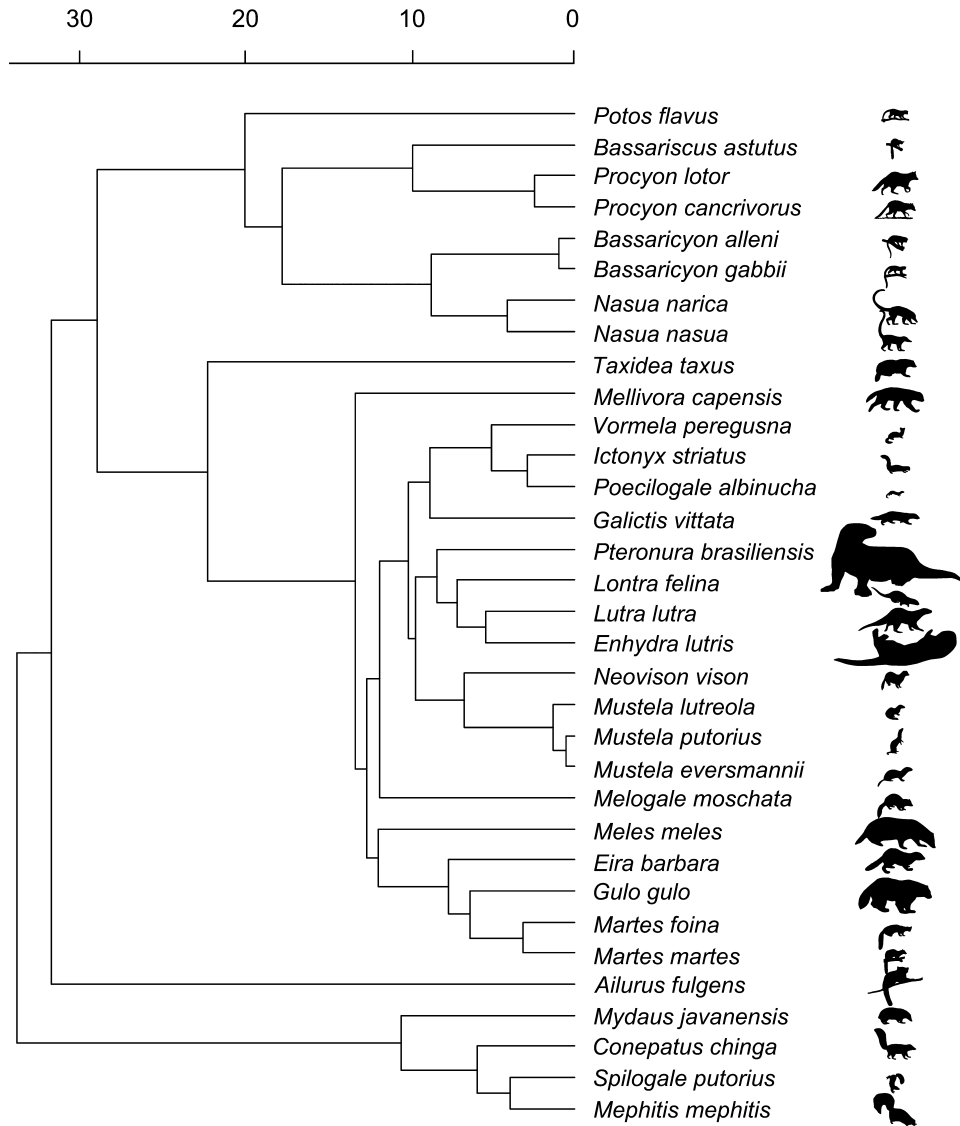
**Figure 1.** The phylogenetic relationships of the musteloid species used in the present study, *sensu* Slater *et al*. (2012). The time scale is in million years.

sliding semilandmarks procedure. Accordingly, we first created a template representing the entire variation of the musteloid data set *sensu* Cornette (2012).

In this procedure, each specimen is first defined by homologous landmark coordinates, which consist of 21 landmarks for the humerus (Fig. 2, Table 2), 19 landmarks for the ulna (Fig. 2, Table 3), and 13 landmarks for the radius (Fig. 2, Table 4). Based on the homologous landmarks, all the sliding-landmarks of the template are warped onto the new specimen at the same time as minimizing the bending energy. Next, the warped sliding-landmarks are projected onto the predefined curves and surfaces of the new specimen. The curves consist of the distal surfaces of the articulation of the humerus and the proximal and distal articulation surface of the radius and ulna (Fig. 2). Finally, spline relaxation must be performed. Both sliding and relaxation are repeated iteratively until the bending energy is minimized. At the end of this procedure, 306 landmarks (21 homologous landmarks and 285 sliding-landmarks) for the humerus, 165 landmarks (13 homologous landmarks and 152 sliding-landmarks) for the radius, and 330 landmarks (19 homologous landmarks and 311 sliding-landmarks) for the ulna are used to describe the shape of each bone and its articulation. After this operation has been performed for each data set, the landmarks of all specimens can be compared using traditional morphometric methods.

**Table 1.** Details of specimens used in analyses with species name, common name, family, number of individuals included (*N*), and mean body mass (kg)

| Species | Common name | Family | *N* | Mean body mass (kg) |
|---|---|---|---|---|
| *Mephitis mephitis* | Striped skunk | Mephitidae | 3 | 3.2 |
| *Spilogale putorius* | Eastern spotted skunk | Mephitidae | 1 | 0.6 |
| *Conepatus chinga* | Molina's hog-nosed skunk | Mephitidae | 1 | 2.9 |
| *Mydaus javanensis* | Sunda stink badger | Mephitidae | 2 | 2.51 |
| *Ailurus fulgens* | Red panda | Ailuridae | 5 | 3.74 |
| *Taxidea taxus* | American badger | Mustelidae | 2 | 4.06 |
| *Mellivora capensis* | Honey badger | Mustelidae | 2 | 8.08 |
| *Vormela peregusna* | Marbled polecat | Mustelidae | 2 | 0.59 |
| *Ictonyx striatus* | Zorilla | Mustelidae | 1 | 0.75 |
| *Poecilogale albinucha* | African striped weasel | Mustelidae | 1 | 0.29 |
| *Galictis vittata* | Greater grison | Mustelidae | 1 | 2.44 |
| *Pteronura brasiliensis* | Giant otter | Mustelidae | 1 | 27.39 |
| *Lontra felina* | Marine otter | Mustelidae | 1 | 4.10 |
| *Lutra lutra* | European otter | Mustelidae | 1 | 8.67 |
| *Enhydra lutris* | Sea otter | Mustelidae | 2 | 29.50 |
| *Neovison vison* | American mink | Mustelidae | 1 | 0.91 |
| *Mustela lutreola* | European mink | Mustelidae | 2 | 0.59 |
| *Mustela putorius* | European polecat | Mustelidae | 2 | 1.03 |
| *Mustela eversmanii* | Steppe polecat | Mustelidae | 1 | 1.7 |
| *Melogale moshata* | Chinese ferret-badger | Mustelidae | 1 | 2.0 |
| *Meles meles* | Eurasian badger | Mustelidae | 3 | 12.94 |
| *Eira barbara* | Tayra | Mustelidae | 1 | 4.39 |
| *Gulo gulo* | Wolwerine | Mustelidae | 2 | 11.13 |
| *Martes foina* | Stone marten | Mustelidae | 3 | 1.8 |
| *Martes martes* | Pine marten | Mustelidae | 2 | 1.14 |
| *Potos flavus* | Kinkajou | Procyonidae | 5 | 2.05 |
| *Procyon cancrivorus* | Crab-eating raccoon | Procyonidae | 3 | 5.0 |
| *Procyon lotor* | Northern raccoon | Procyonidae | 5 | 6.17 |
| *Nasua narica* | White-nosed coati | Procyonidae | 4 | 4.0 |
| *Nasua nasua* | South American coati | Procyonidae | 4 | 4.5 |
| *Bassaricyon alleni* | Allen's olingo | Procyonidae | 3 | 1.25 |
| *Bassaricyon gabbii* | Bushy-tailed olingo | Procyonidae | 3 | 1.235 |
| *Bassariscus astutus* | Ringtail | Procyonidae | 7 | 0.84 |

Once all landmark data were obtained, a generalized Procrustes superimposition (Rohlf & Slice, 1990) was performed on the point coordinates using RMORPH (Baylac, 2012) in R (R Development Core Team, 2011). A principal component (PC) analysis on the shape data was performed to evaluate the distribution of species in morphospace. The visualizations of shapes at the extreme of each axis were performed using both EVAN TOOLBOX (http://www.evan.at) (3D thin-plate spline visualizations) and a vector-based visualization of the change in conformation using GEOMAGIC STUDIO (http://www.geomagic.com).

PHYLOGENETIC SIGNAL

To estimate the phylogenetic signal in long bone forelimb shape, we used a randomization test *sensu* Blomberg, Garland & Ives (2003). A *K*-statistic was calculated for the first six PCs of our sample using the 'picante' library in R (Kembel *et al.*, 2010). The *K*-statistic is a simple comparison of the phylogenetic signal observed in our shape data relative to the phylogenetic signal observed for a trait under Brownian motion on a given phylogeny (topology and branch lengths). To calculate this *K*-statistic, we used our shape descriptors and the recently published time-calibrated phylogeny of caniform carnivorans from Slater, Harmon & Alfaro (2012). The tree uses the family-level phylogeny of Carnivora from Eizirik *et al.* (2010) as a backbone, with time-calibrated molecular phylogenies for each family appended to it. Full details of the phylogenetic reconstruction are provided in Slater *et al.* (2012). For our analyses, we pruned the tree so that only species represented in
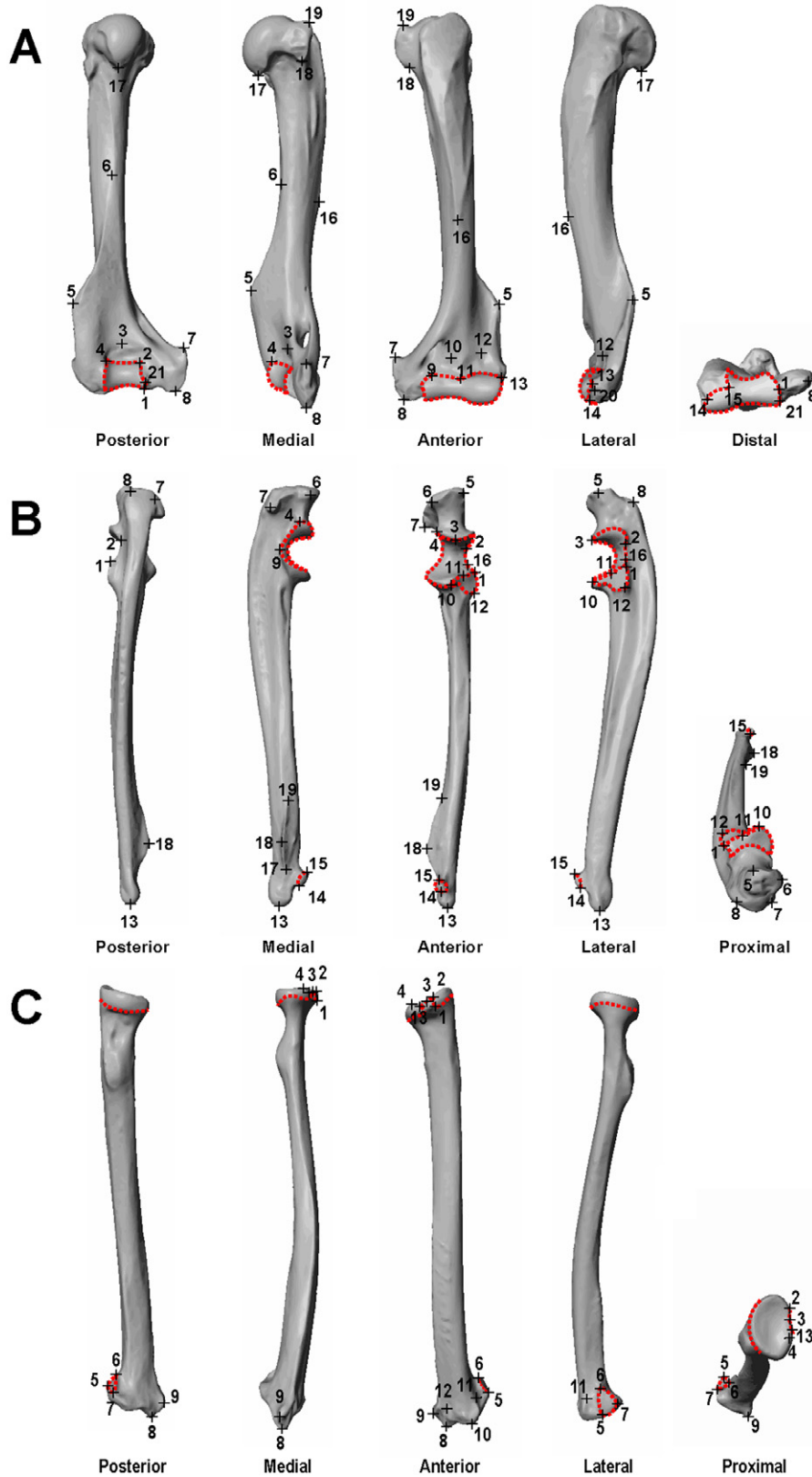
**Figure 2.** Landmarks used in the analyses quantifying shape variation on the forelimb bones. A, humerus. B, ulna. C, radius. Black crosses represent landmarks; red-dashed lines represent outlines used for the surface analyses of the articulations of each bone.

**Table 2.** Definition of the landmarks of the humerus used in the geometric morphometric analysis

| Landmark | Definition |
|---|---|
| 1 | Most medio-distal point of the caudal part of the trochlea |
| 2 | Most medio-proximal point of the caudal side of the trochlea |
| 3 | Point of maximum of curvature of the olecranon fossa |
| 4 | Most latero-proximal point of the caudal side of the trochlea |
| 5 | Point of maximum of convexity of the lateral epicondylar crest |
| 6 | Point of insertion of the lateral epicondylar crest on the diaphyse |
| 7 | Most proximal tip of the medial epicondyle |
| 8 | Most distal tip of the medial epicondyle |
| 9 | Most medio-proximal point of the cranial side of the trochlea |
| 10 | Point of maximum of curvature of the coronoid fossa |
| 11 | Most proximo-anterior point of contact between the trochlea and the capitulum |
| 12 | Point of maximum of curvature of the radial fossa |
| 13 | Most latero-proximal point of the cranial side of the capitulum |
| 14 | Most disto-lateral point of the capitulum |
| 15 | Most distal point of contact between the trochlea and the capitulum |
| 16 | Most distal point of the deltopectoral crest |
| 17 | Tip of the lesser tuberosity |
| 18 | Most proximo-medial point of the greater tuberosity |
| 19 | Most disto-medial point of the greater tuberosity |
| 20 | Most latero-distal point of the cranial side of the capitulum |
| 21 | Point of maximum of concavity of the caudo-medio-distal part of the trochlea |

**Table 3.** Definition of the landmarks of the ulna used in the geometric morphometric analysis

| Landmark | Definition |
|---|---|
| 1 | Most lateral point of contact between the trochlear notch and the radial notch |
| 2 | Most proximo-lateral point of the incisure of the trochlear notch |
| 3 | Point of maximum of concavity of the proximal part of the trochlear notch |
| 4 | Most proximo-medial point of the incisure of the trochlear notch |
| 5 | Most palmar-lateral point of olecranon process |
| 6 | Most palmar-medial point of olecranon process |
| 7 | Most dorsal-medial point of olecranon process |
| 8 | Most dorsal-lateral point of olecranon process |
| 9 | Point where the most medial part of the coronoid process meets the most medio-distal part of the trochlear notch |
| 10 | Most anteriorl point of contact between the trochlear notch and the radial notch |
| 11 | Point of maximum of concavity between the radial notch and the trochlear notch |
| 12 | Most latero-distal point of insertion of the radial notch |
| 13 | Tip of the styloid process |
| 14 | Most distal point of the articular facet that articulates with the radius |
| 15 | Most proximal point of the articular facet that articulates with the radius |
| 16 | Point where the proximo-lateral part of the coronoid process meets the lateral part of the trochlear notch |
| 17 | Most distal point of insertion of the medial epicondylar crest on the diaphysis |
| 18 | Point of maximum of curvature of the medial epicondylar crest |
| 19 | Most proximal point of insertion of the medial epicondylar crest on the diaphysis |

our dataset remained (Fig. 1). The higher the *K*-value is, the stronger the phylogenetic signal. A *K*-value of 1 corresponds to character evolution under Brownian motion and indicates some degree of phylogenetic signal. A *K*-value greater than 1 indicates a strong phylogenetic signal, which means that traits are conserved within the phylogeny. Conversely, a *K*-value close to 0 means that phylogenetic signal is weak, indicating strong morphological convergence.

INDEPENDENT CONTRAST ANALYSIS

Because species share part of their evolutionary history, they cannot be treated as independent data points. Thus, we explored the relationships between body mass and the shape of the forelimb elements by calculating independent contrasts (Felsenstein, 1985), regressing shape onto body mass. Body mass is a good predictor because of its differential scaling and the mechanical constraints that it imposes on the forelimb skeleton. Body masses were obtained from the literature (Myers *et al.*, 2012) and $\log_{10}$ transformed to meet assumptions of normality and homoscedasticity. Species mean shapes were calculated for each element using the first four PCs of the humerus, and

**Table 4.** Definition of the landmarks of the radius used in the geometric morphometric analysis

| Landmark | Definition |
|---|---|
| 1 | Most disto-lateral point of anterior side of the ulnar facet |
| 2 | Most proximo-lateral point of anterior side of the ulnar facet |
| 3 | Point of maximum of concavity of the anterior part of the fovea |
| 4 | Tip of the fovea |
| 5 | Most disto-medial point of the distal articular facet with the ulna |
| 6 | Most proximal point of curvature of the distal articular facet with the ulna |
| 7 | Most disto-lateral point of the distal articular facet with the ulna |
| 8 | Distal tip of the styloid process |
| 9 | Medial tip of the styloid process |
| 10 | Most disto-lateral point of the dorsal side of the radius |
| 11 | Most proximal point of the groove for extensor digitorium and extensor indicis |
| 12 | Most proximo point of groove for extensor carpi radialis longus and brevis |
| 13 | Most disto-medial point of the anterior side of the ulnar facet |

**Table 5.** Results of $K$-statistics and their associated $P$-value as calculated for the first four principal shape components of the humerus, the first three principal shape components of the ulna, and the first three principal shape components of the radius

|  | $K$ | $P$-value |
|---|---|---|
| Humerus |  |  |
| **PC1** | **0.65** | **0.0009** |
| **PC2** | **0.47** | **0.003** |
| PC3 | 0.24 | 0.25 |
| PC4 | 0.27 | 0.089 |
| Ulna |  |  |
| ***PC1*** | ***1.12*** | ***0.0009*** |
| PC2 | 0.24 | 0.22 |
| **PC3** | 0.81 | **0.0009** |
| Radius |  |  |
| **PC1** | **0.87** | **0.0009** |
| **PC2** | **0.93** | **0.0009** |
| PC3 | 0.38 | 0.014 |

Principal components with a significant phylogenetic signal ($\alpha < 0.05$) are shown in bold. Components with $K$-values > 1 are shown in bold and italic.

the first three PCs of the ulna and radius. The phylogenetic framework used to conduct this analysis is the same that we present above with respect to the phylogenetic signal. To fit the assumption of independent contrasts, we verified in PDAP (Midford, Garland & Maddison, 2005) of MESQUITE (Maddison & Maddison, 2011) that our branch lengths are indeed adequate for all traits. When not appropriate, they were transformed using Nee transformation (Purvis, 1995). Next, the standardized contrasts of all shape variables were regressed against the standardized contrasts of body mass through the origin using a simple ordinary least squares regression model.

## RESULTS

### BODY MASS

Among the species of musteloids included in our data set, the mean body mass varied from 0.29 kg for the African striped weasel (*Poecilogale albinucha*) to 29.5 kg for the sea otter (*E. lutris*; Table 1).

### GEOMETRIC MORPHOMETRICS

The first four PCs of the humerus accounted for 69.88% of the variance. The overall distribution of the

different taxa in the morphospace defined by the first and second axis (Fig. 3A) showed a more extensive distribution of the mustelids in morphospace compared to procyonids, which clustered with the ailurid on the negative part of the first axis. The first three PC axes for the ulna accounted for 70.1% of the overall shape variation. The morphospace as defined by the scatter plot of the first and second axis (Fig. 3B) also showed a wider distribution of mustelids compared to procyonids that tend to be clustered with the ailurid along the negative part of the first axis. Mephitids form a cluster inside the mustelid group, in the middle of the morphospace. The first three PCs of the radius accounted for 77.82% of the total shape variation. The overall distribution of taxa on the first and third axis (Fig. 3C) was similar to those of the humerus and ulna.

### PHYLOGENETIC SIGNAL

Table 5 shows the values for the $K$-statistic and its associated significance levels for each forelimb long bone. The $K$-statistic calculated for the first four PCs of the humerus is lower than 1, although the randomization tests showed a significant phylogenetic signal for the first two PCs of shape variation for the humerus (PC1, $P = 0.0009$; PC2, $P = 0.003$). The $K$-statistic calculated for the first PC of the ulna is higher than 1 (PC1, $K = 1.12$), which indicates a phylogenetic signal in the shape of the ulna. The
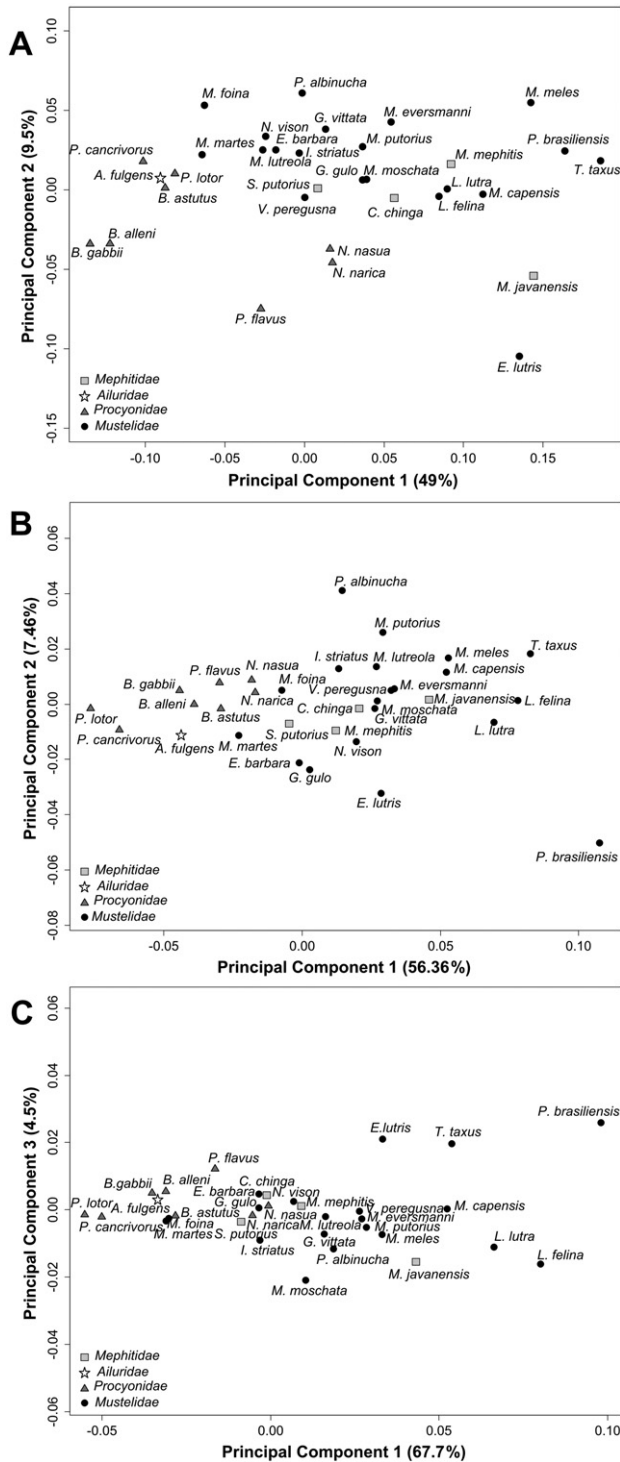
**Figure 3.** Results of a principal components analysis performed on the morphometric data. A, humerus; scatter plot illustrating the position of different species on the first two principal components. B, ulna; scatter plot illustrating the position of different species on the first two principal components. C, radius; scatter plot illustrating the position of different species on the axes one and three. The family of each species is represented by a black dot for mustelids, a dark grey triangle for procyonids, a light grey square for mephitids, and a white star for ailurids.

**Table 6.** Results of the regression analysis comparing the standardized contrasts of shape against the standardized contrasts of $\log_{10}$ body mass for the first four principal shape components of the humerus, the first three principal shape components of the ulna, and the first three principal shape components of the radius

| Variable | R | P-value |
|---|---|---|
| **Humerus PC1** | **0.65** | **0.000041** |
| Humerus PC2 | 0.24 | 0.17 |
| Humerus PC3 | 0.015 | −0.93 |
| Humerus PC4 | 0.3 | 0.087 |
| Ulna PC1 | 0.23 | 0.19 |
| **Ulna PC2** | **0.47** | **0.005** |
| Ulna PC3 | 0.059 | 0.74 |
| Radius PC1 | 0.276 | 0.12 |
| Radius PC2 | 0.14 | 0.43 |
| **Radius PC3** | **0.42** | **0.014** |

*R* indicates the correlation between the two variables of interest based on regressions forced through the origin, and principal components with significant correlations are shown in bold.

*K*-statistic calculated for the first three PCs of the radius is lower than 1, although the randomization test showed a significant phylogenetic signal for the first two PCs of shape variation for the radius (PC1, $P = 0.0009$; PC2, $P = 0.0009$). These results highlight the importance of performing phylogenetic corrections on our data, and also suggest that forelimb shape is at least partially constrained by phylogeny, albeit with the effect being relatively minor.

INDEPENDENT CONTRAST ANALYSIS

The results of the regression analyses (Fig. 4, Table 6) indicated that the standardized contrasts of shape (first PC for the humerus, the second PC for the ulna, and the third PC for the radius) are correlated with the standardized contrasts of body mass. This result indicated that body mass evolution goes hand in hand with the evolution of the shape of the humerus as

*K*-statistic is lower than 1 for the other PCs, although it approaches 1 for PC3 ($K = 0.81$). The randomization test showed a significant phylogenetic signal for the first and the third PCs (PC1, $P = 0.0009$; PC3, $P = 0.0009$) of shape variation for the ulna. The
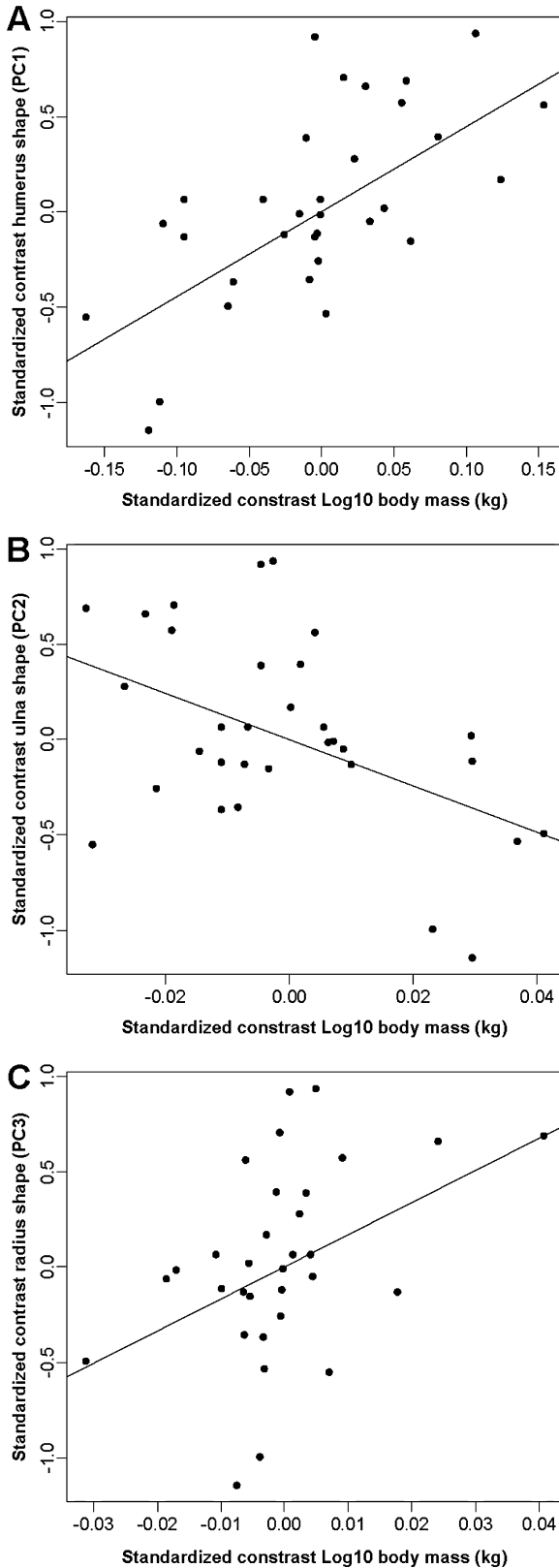
**Figure 4.** Results of the correlation between the standardized contrasts of humeral shape with the standardized contrasts of body mass (A); the standardized contrasts of ulnar shape with the standardized contrasts of body mass (B); and the standardized contrasts of radial shape with the standardized contrasts of body mass (C).

defined by the first PC, the ulna as defined by the second PC, and the radius as defined by the third PC.

### RELATIONSHIP BETWEEN BODY MASS AND FORELIMB LONG BONES SHAPE

Shape variation of the humerus as described by the first PC shows that species with a low body mass (Fig. 5) are generally characterized by a gracile humerus with a relatively small distal articulation, a capitulum that is relatively broader in comparison to the trochlea, a relatively narrow and concave trochlea, a relatively straight medial lip of the trochlea, a relatively short medial epicondyle, and a relatively small lateral epicondylar crest. By contrast, humeri of species with a large body mass are relatively more robust and have a relatively broad distal articulation with a smaller capitulum in comparison to the trochlea, a medial lip of the trochlea that is oriented more medially, a relatively large medial epicondyle, and a relatively prominent lateral epicondylar crest.

Ulnar shape changes associated with body mass variation suggest that species with a large body mass on the negative part of the PC2 axis are characterized by a relatively curved ulna with a relatively curved and anteriorly oriented olecranon process, a relatively broad proximal radial and trochlear notches, a constriction of the trochlear notch being relatively well-marked, a relatively short and flat medial epicondylar crest with a more proximal insertion on the diaphysis that is higher than the distal radial facet, and a relatively broad distal radial notch. In contrast, species with a lower body mass fall on the positive part of the axis and correspondingly display the opposite morphology.

Shape changes of the radius associated with species with a low body mass situated on the negative end of third PC (Fig. 5) are characterized by a relatively thin proximal articulation with a radial head that is oval-shaped, a relatively more concave anterior part of the fovea with a relatively prominent capitular eminence, and a posterior border of the proximal ulnar facet that is oval. However, they have an anterior border that is relatively concave and asymmetric with a relatively broad interruption of its rim, an antero-medial part of the proximal ulnar facet that is relatively thin, a distal articulation that is relatively small, and a relatively symmetrical distal epiphysis
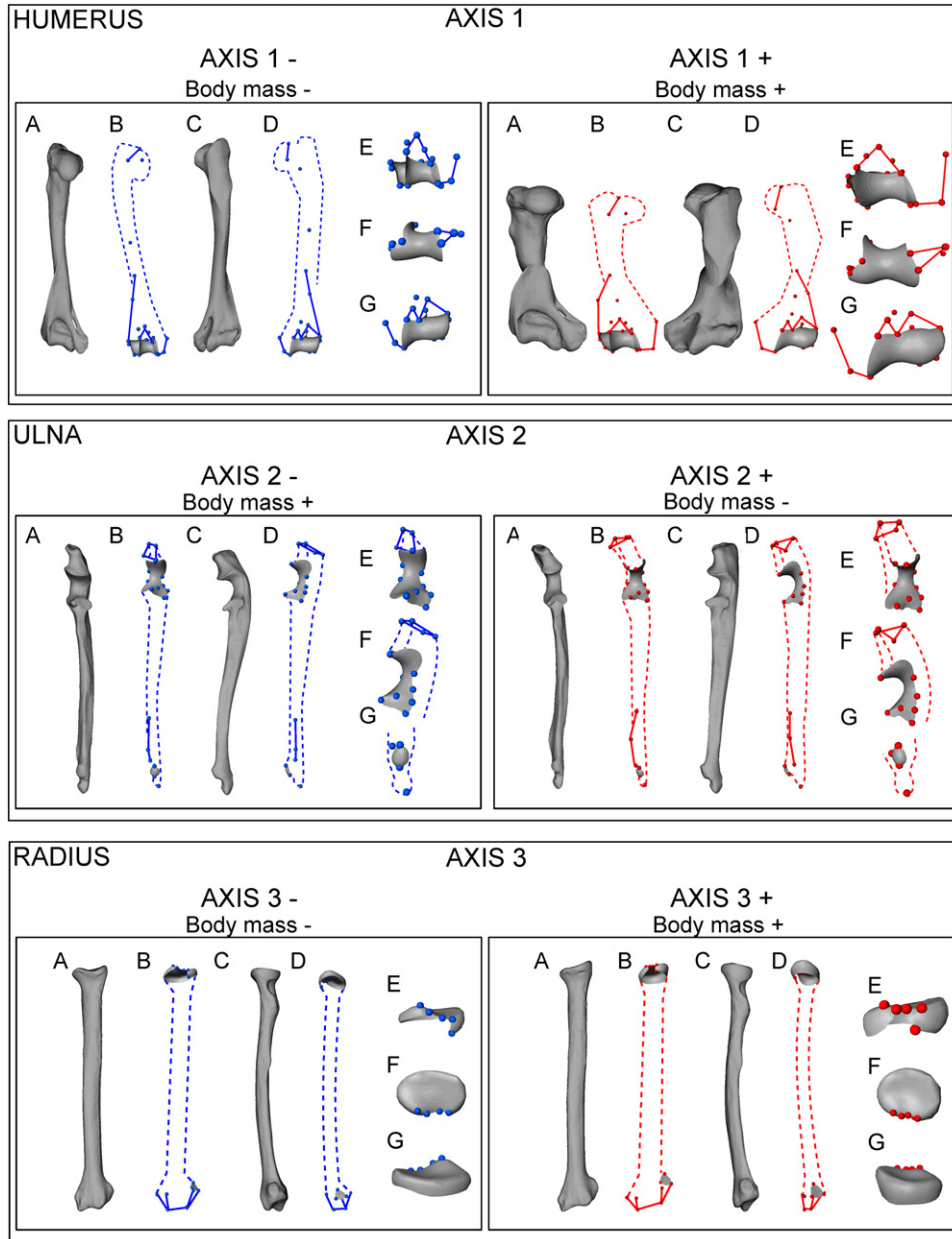
**Figure 5.** Shape change of forelimb elements observed in species with low (body mass –) and high (body mass +) body mass. Humerus: posterior view obtained through three-dimensional (3D) thin-plate spline visualizations (A); posterior view;, anterior view using 3D thin-plate spline visualizations (C); anterior view (D); close up of the distal articulation in posterior view (E); distal view (F); close up of the distal articulation in anterior view (G). Ulna: anterior view obtained using 3D thin-plate spline visualizations (A); anterior view (B); lateral view obtained using 3D thin-plate spline visualizations (C); lateral view (D); close up of the proximal articulation in anterior view (E); close up of the proximal articulation in lateral view (F); close up of the distal articulation in anterior view (G). Radius: anterior view obtained using 3D thin-plate spline visualizations (A); anterior view (B); lateral view obtained using 3D thin-plate spline visualizations (C); lateral view (D); close up of the proximal articulation in anterior view (E); proximal view (F); close up of the proximal articulation in posterior view (G). Dots and grey surfaces represent landmarks; lines represent real links between landmarks; dashed-lines represent a schematic representation of the bone.

with a prominent medial styloid process at the same level than the distal ulnar notch. By contrast, species with a large body mass falling on the positive part of the axis display a relatively broad proximal articulation with a radial head that is round-shaped, a relatively more flat anterior part of the fovea with a relatively flat capitular eminence, a relatively broad and round ulnar facet, an antero-medial part of the proximal ulnar facet that is relatively broad and symmetric with a small interruption of its rim, a distal articulation that is relatively big, and a relatively asymmetrical distal epiphysis with a prominent medial styloid process lower than the distal ulnar notch.

## DISCUSSION

The results of the forelimb long bones shape analysis in musteloid carnivorans show that there is no clustering of species with low or high body mass in morphospace (Fig. 3). The distribution of the species thus appears to be driven by other factors (e.g. phylogeny or locomotor ecology). The calculation of phylogenetic signal indicates that shape is at least partially constrained by phylogeny, which may explain part of the distribution of the species in morphospace with distinct groupings of mustelids, procyonids, and, in some cases, mephitids (Fig. 3).

The results of the regression analyses (Table 6) indicate that the standardized contrasts of the shape of the forelimb long bones are correlated with the standardized contrasts of body mass, even though the regression coefficients are relatively low. Our analyses showed a positive correlation between the standardized contrasts of humeral and radial shape versus the standardized contrasts of body mass (Fig. 4). By contrast, a negative correlation between the standardized contrasts of ulnar shape and the standardized contrasts of body mass was observed (Fig. 4). These low coefficients suggest that factors other than body mass, such as phylogeny, as well as possibly locomotor style, drive the evolution of forelimb long bone shape in this clade. Indeed, variation in life-style (aquatic, terrestrial, arboreal) will likely induce variation in locomotor ecology and thus gravitational constraints imposed by body mass will likely differ for aquatic versus terrestrial species. It should also be recognized that discriminating between the effects of body mass and certain ecologies may not always be straightforward because both may put similar functional demands on the forelimb skeleton. For example, the large and rounded radial head may be associated both with a more efficient force transmission, as well as improved lower forearm mobility (i.e. facilitating pronation and supination). Additionally, smaller species often show a more crouched type of locomotion that will affect the nature in which the forelimbs are loaded during locomotion. Yet, our results also show that the evolution of a greater body mass goes hand in hand with the evolution of a specific long bone shape (Fig. 5).

The shape associated with the humerus of species with a large body mass (Fig. 5) is robust with a large distal articulation. This type of morphology was suggested to be a consequence of the large body mass in several previous studies (Biewener, 1983; Andersson, 2004; Meachen-Samuels & Van Valkenburgh, 2009). Indeed, a large articulation will increase the surface area and therefore will better distribute the load, which is transferred through the articulation (Ruff, 1988; Meachen-Samuels & Van Valkenburgh, 2009). Moreover, the trochlea is large, whereas the capitulum is really short in species with a large body mass. This type of morphology suggests that the humero-ulnar joint plays a significant role in load bearing and load transmission at the elbow joint, which is common in quadrupedal mammals (Szalay & Dagosto, 1980; Rose, 1988; Sargis, 2002; Salton & Sargis, 2008).

The shape associated with the radius of species with a large body mass (Fig. 5) is rather robust with a large radial head. This radial morphology has been interpreted as being important with respect to transferring the load from the upper part onto the lower part of the forelimb (Taylor, 1989; Sargis, 2002; Argot, 2003). Moreover, the large and broad ulnar notch appears to provide a larger area of contact with the ulna that will facilitate the distribution of forces between both segments of the forearm (Rose, 1988; Patel, 2005). The distal part of the radius is large in species with a large body mass with a styloid process that is well developed in comparison to species with a low body mass. Potentially, these features could be related to the fact that the distal part of the radius plays an important role in load-bearing at the proximal part of the wrist, thus stabilizing it by restricting its degree of movement (Salton & Sargis, 2008).

The shape associated with the ulna of species with a large body mass (Fig. 5) is curved, with an olecranon process that is oriented anteriorly. This morphology has been previously interpreted as providing an increased mechanical advantage for the forearm extensors when the forearm is in flexion. Indeed, the insertion of the triceps muscle on the olecranon process gives it an increased mechanical advantage when the forearm is flexed (Argot, 2001; Szalay & Sargis, 2001; Sargis, 2002; Candela & Picasso, 2008).

## CONCLUSIONS

To conclude, our results at least partly confirm our predictions and demonstrate that body mass evolution does indeed affect the evolution of forelimb long bone shape in musteloid carnivorans. Interestingly,

humeral and radial shape appear to be better adapted for load bearing and load transmission than is the shape of the ulna, with heavier species displaying a shorter and more robust humerus and radius with a wider articulation surface. Nevertheless, as suggested by the relatively low regression coefficient of the phylogenetic contrasts, body mass is not the only (or even primary) driver of forelimb long bone shape evolution. Consequently, it would be interesting to study the influence of, for example, locomotor behaviour or lifestyle on the morphology of the forelimb. In addition, it would be also interesting to perform explicit biomechanical studies, such as finite element analysis, to explore how the the articular shapes described in the present study may help dissipate forces in the joints of animals with increased body mass.

## ACKNOWLEDGEMENTS

## REFERENCES

**Andersson K. 2004.** Predicting carnivoran body mass from a weight-bearing joint. *Journal of Zoology* **262:** 161–172.

**Argot C. 2001.** Functional-adaptive anatomy of the forelimb in the Didelphidae, and the paleobiology of the Paleocene marsupials *Mayulestes ferox* and *Pucadelphys andinus*. *Journal of Morphology* **247:** 51–79.

**Argot C. 2003.** Funtional adaptations of the postcranial skeleton of two Miocene borhyaenoids (Mammalia, Metatheria), *Borhyaena* and *Prothylacinus*, from South America. *Paleontology* **46:** 1213–1267.

**Baylac M. 2012.** *Rmorph: an R geometric and multivariate morphometrics library*. Available from the author: baylac@mnhn.fr.

**Bertram JE, Biewener AA. 1990.** Differential scaling of the long bones in the terrestrial carnivora and other mammals. *Journal of Morphology* **204:** 157–169.

**Biewener AA. 1983.** Locomotory stresses in the limb bones of two small mammals: the ground squirrel and chipmunk. *Journal of Experimental Biology* **103:** 131–154.

**Biewener AA. 1989.** Scaling body support in mammals: limb posture and muscle mechanics. *Science* **245:** 45–48.

**Biewener AA. 2005.** Biomechanical consequences of scaling. *Journal of Experimental Biology* **208:** 1665–1676.

**Blob RW, Biewener AA. 2001.** Mechanics of limb bone loading during terrestrial locomotion in the green iguana (*Iguana iguana*) and American alligator (*Alligator mississippiensis*). *Journal of Experimental Biology* **204:** 1099–1122.

**Blomberg SP, Garland T Jr, Ives AR. 2003.** Testing for phylogenetic signal in comparative data: behavioural traits are more labile. *Evolution* **57:** 717–745.

**Bookstein FL. 1997.** Landmark methods for forms without landmarks: morphometrics of group differences in outline shape. *Medical Image Analysis* **1:** 225–243.

**Bookstein FL, Green WDK. 2002.** *Users manual, EWSH3.19*. Available at: http://brainmap.stat.washington.edu/edgewarp/

**Candela AM, Picasso MBJ. 2008.** Functional anatomy of the limbs of Erethizontidae (Rodentia, Caviomorpha): indicators of locomotor behavior in Miocene porcupines. *Journal of Morphology* **269:** 552–593.

**Christiansen P. 1999.** Scaling of the limb long bones to body mass in terrestrial mammals. *Journal of Morphology* **239:** 167–190.

**Cornette R. 2012.** Form and function: modularity and disparity of the feeding apparatus of *Crocidura russula* (Soricomorpha, Soricidae). PhD dissertation, Muséum National d'Histoire Naturelle, Paris, France.

**Day LM, Jayne BC. 2007.** Interspecific scaling of the morphology and posture of the limbs during the locomotion of cats (Felidae). *Journal of Experimental Biology* **210:** 642–654.

**Eizirik E, Murphy WJ, Koepfli KP, Johnson WE, Dragoo JW, Wayne RK, O'Brien SJ. 2010.** Pattern and timing of diversification of the mammalian order Carnivora inferred from multiple nuclear gene sequences. *Molecular Phylogenetics and Evolution* **56:** 49–63.

**Evans HE. 1993.** *Miller's anatomy of the dog*, 3rd edn. Philadelphia, PA: WB Saunders.

**Felsenstein J. 1985.** Phylogenies and the comparative method. *American Naturalist* **125:** 1–15.

**Gunz P, Mitteroecker P, Bookstein FL. 2005.** Semilandmarks in three dimensions. In: Slice SE, ed. *Modern morphometrics in physical anthropology*. New York, NY: Kluwer Academic/Plenum Publishers, 73–98.

**Heinrich RE, Biknevicius AR. 1998.** Skeletal allometry and interlimb scaling. *Journal of Morphology* **235:** 121–134.

**Jenkins FA. 1973.** The functional anatomy and evolution of

the mammalian humero-ulnar articulation. *American Journal of Anatomy* **137:** 281–297.

**Kembel SW, Cowan PD, Helmus MR, Cornwell WK, Morlon H, Ackerly DD, Blomberg SP, Webb CO. 2010.** Picante: R tools for integrating phylogenies and ecology. *Bioinformatics* **26:** 1463–1464.

**Maddison WP, Maddison DR. 2011.** *Mesquite: a modular system for evolutionary analysis*, Version 2.75. Available at: http://mesquiteproject.org

**Meachen-Samuels J, Van Valkenburgh B. 2009.** Forelimb indicators of prey-size preference. *Journal of Morphology* **270:** 729–744.

**Midford PE, Garland JT, Maddison WP. 2005.** *PDAP package of mesquite*, Version 1.07. Available at: http://mesquiteproject.org/pdap_mesquite/index.html

**Myers P, Espinosa R, Parr CS, Jones T, Hammond GS, Dewey TA. 2012.** *The animal diversity web* (online). Available at: http://animaldiversity.org

**Patel BA. 2005.** The hominoid proximal radius: re-interpreting locomotor behaviors in early hominins. *Journal of Human Evolution* **48:** 415–432.

**Purvis A. 1995.** A composite estimate of primate phylogeny. *Philosophical Transactions of the Royal Society of London Series B, Biological Sciences* **348:** 405–421.

**R Development Core Team. 2011.** R: *a language and environment for statistical computing*. Vienna: R Foundation for Statistical Computing, ISBN 3-900051-07-0. Available at: http://www.R-project.org

**Reynolds TR. 1985.** Stresses on the limbs of quadrupedal primates. *American Journal of Physical Anthropology* **67:** 351–362.

**Rohlf FJ, Slice D. 1990.** Extensions of the procrustes method for the optimal superimposition of landmarks. *Systematic Zoology* **39:** 40–59.

**Rose MD. 1988.** Another look at the anthropoid elbow. *Journal of Human Evolution* **17:** 193–224.

**Rubin CT, Lanyon LE. 1982.** Limb mechanics as a function of speed and gait: a study of functional strains in the radius and tibia of horse and dog. *Journal of Experimental Biology* **101:** 187–211.

**Ruff CB. 1988.** Hindlimb articular surface allometry in Hominoidea and Macaca, with comparisons to diaphyseal scaling. *Journal of Human Evolution* **17:** 687–714.

**Ruff CB, Runestad JA. 1992.** Limb bone structural adaptations. *Annual Review of Anthropology* **21:** 407–433.

**Salton JA, Sargis EJ. 2008.** Evolutionary morphology of the Tenrecoidea (Mammalia) forelimb skeleton. In: Sargis EJ, Dagosto M, eds. *Mammalian evolutionary morphology: a tribute to Frederick S. Szalay*. Dordrecht: Springer, 51–71.

**Sargis EJ. 2002.** Functional morphology of the forelimb of tupaiids (Mammalia, Scandentia) and its phylogenetic implications. *Journal of Morphology* **253:** 10–42.

**Sato JJ, Wolsan M, Minami S, Hosoda T, Sinaga MH, Hiyama K, Yamaguchi Y, Suzuki H. 2009.** Deciphering and dating the red panda's ancestry and early adaptive radiation of Musteloidea. *Molecular Phylogenetics and Evolution* **53:** 907–922.

**Sato JJ, Wolsan M, Prevosti FJ, D'Elía G, Begg C, Begg K, Hosoda T, Campbell KL, Suzuki H. 2012.** Evolutionary and biogeographic history of weasel-like carnivorans (Musteloidea). *Molecular Phylogenetics and Evolution* **63:** 745–757.

**Schmidt-Nielson K. 1984.** *Scaling: why is animal size so important?* Cambridge: Cambridge University Press.

**Slater GJ, Harmon LJ, Alfaro ME. 2012.** Integrating fossils with molecular phylogenies improves inference of trait evolution. *Evolution* **66:** 3931–3944.

**Szalay FS, Dagosto M. 1980.** Locomotors adaptations as reflected on the humerus of Paleogene primates. *Folia Primatologica* **34:** 1–45.

**Szalay FS, Sargis E. 2001.** Model-based analysis of postcranial osteology of marsupials from the Paleocene of Itabora? (Brasil) and the phylogenetics and biogeography of Metatheria. *Geodiversitas* **23:** 139–302.

**Taylor ME. 1989.** Locomotor adaptations by carnivores. In: Gittleman JL, ed. *Carnivore behavior, ecology, and evolution*. Ithaca, NY: Comstock/Cornell University Press, 382–409.

**Thomason JJ. 1985.** Estimation of locomotory forces and stresses in the limb bones of recent and extinct equids. *Paleobiology* **11:** 209–220.

**Wiley DF, Amenta N, Alcantara DA, Ghosh D, Kil YJ, Delson E, Harcourt-Smith W, Rohlf FJ, St John K, Hamann B. 2005.** Evolutionary morphing. In: *Proceedings of IEEE visualization 2005 (VIS'05)*, 23–28 October 2005. Minneapolis, 431–438.

## SUPPORTING INFORMATION

Additional Supporting Information may be found in the online version of this article at the publisher's web-site:

**Table S1.** Specimens used in analyses. Institutional abbreviations: CG, Muséum National d'Histoire Naturelle Catalogue Générale, Paris; MCZ, Harvard Museum of Comparative Zoology, Cambridge, Massachusetts; NMB, Natuhistorishes Museum Basel, Basel; USNM, the Smithsonian National Museum of Natural History, Washington, District of Columbia. Sex abbreviations are follows: F: female; M: male; U: unknown.